Relevance of ERA40 dynamical downscaling for modeling deep convection in the North-Western Mediterranean Sea

Marine J. Herrmann, Samuel Somot

Relevance of ERA40 dynamical downscaling for modeling deep convection in the Mediterranean Sea

Marine J. Herrmann

Laboratoire d'Aérologie, CNRS, Université Paul Sabatier, Toulouse, France

Samuel Somot

Centre National de Recherches Météorologiques, Météo-France, Toulouse,

France

Marine Herrmann, Laboratoire d'Aérologie, 14 av. Edouard Belin, 31400 Toulouse, FRANCE,

marine.herrmann@m4x.org

A strong open-ocean convection event was observed in the Northwestern Mediterranean sea during the 1986-87 winter. This period was used as a case study to evaluate the impact of the spatial resolution of atmospheric forcing on deep convection modeling. Twin numerical experiments were performed with an oceanic model forced by atmospheric forcing sets with different resolutions. A low resolution atmospheric forcing extracted from the ERA40 reanalysis was compared with a high resolution forcing produced by a dynamical downscaling of ERA40. A high resolution climate model spectrally driven by ERA40 fields for the large scales provided the dynamical downscaling dataset covering the 1958-2001 period. The oceanic simulation performed under low resolution meteorological forcing did not reproduce the observed convection. The simulation performed under high resolution forcing correctly reproduced the convection event. This was principally due to the enhancement of spatial and temporal meteorological extremes under the high resolution forcing.

1. Introduction

Deep convection is a key process for the Northwestern Mediterranean sea (NWMS) oceanic circulation and ecosystem. This process shows high interannual variability whose understanding and modeling still need to be improved. Atmospheric conditions, namely strong northerly winds and significant heat loss, are the principal drivers of winter deep convection, and hence account for much of its variability. These atmospheric conditions (Tramontane, Mistral, cyclogenesis of the Gulf of Genoa, ...) are themselves mainly driven by the local orography of the Mediterranean coast (Pyrénées, Alpes, Massif Central, Rhône valley) that induces physical processes such as lee cyclogenesis or wind channeling. It is therefore essential to use an appropriate atmospheric forcing method when performing numerical studies of deep convection. Currently, high resolution atmospheric fluxes are only available for recent years (ECMWF analysis at 50 km resolution available since 1990, used by *Béranger et al.* [2005]).

The 1986-87 winter was cold and windy in the NWMS, leading to a strong bottom open-ocean convection event [*Mertens and Schott*, 1998] that was monitored during a specific campaign (MEDOC87, reported by *Schott and Leaman* [1991] and *Leaman and Schott* [1991], hereafter SL91 and LS91). This period is therefore particularly appropriate to evaluate the capacity of an oceanic model to represent deep convection [*Demirov and Pinardi*, 2007; *Herrmann et al.*, 2008] as well as the impact of atmospheric forcing resolution on this modeling problem, as suggested in those studies.

We carried out a spectral dynamical downscaling of the ERA40 reanalysis [*Simmons and Gibson*, 2000] to obtain a high resolution long-term dataset following the observed

chronology over the 1958-2001 period. Twin numerical simulations of the 1986-87 winter were performed using an eddy-resolving oceanic model forced at the surface by two sets of atmospheric fluxes: the first directly extracted from ERA40 and the second produced by the downscaling. The objectives of this study were to evaluate the influence of the atmospheric forcing spatial resolution on convection modeling and to underline the relevance of the downscaled ERA40 atmospheric fluxes in the framework of realistic oceanic modeling.

2. Dynamical downscaling of the ERA40 reanalysis

ERA40 is widely used to analyse the variability of oceanic and atmospheric circulation over Europe during the last decades, in particular for the period before the 1990s, i.e. prior to the high resolution ECMWF analysis. Covering the 1958-2001 period with a spatial resolution of $\sim$125 km, this reanalysis is indeed one of the most homogeneous, high-resolution and long-term databases available to force ocean models. Moreover, since the data assimilation system constrains the temporal behavior of the atmospheric flow, synoptic events follow the observed chronology. It was however suggested that its resolution is not sufficient to realistically simulate the formation of the deep waters involved in the Mediterranean thermohaline circulation [*Josey*, 2003; *Demirov and Pinardi*, 2007; *Herrmann et al.*, 2008]. We tested this hypothesis by increasing the ERA40 resolution with a downscaling method.

2.1. The downscaling method

Several statistical or dynamical methods aimed at downscaling a reanalysis were developed. *Sotillo et al.* [2005] performed a dynamical downscaling of the NCEP reanalysis

[*Kalnay et al.*, 1996] over the Mediterranean basin with a limited area model forced at its lateral boundaries and with spectral nudging over the central area. We also applied a dynamical downscaling based on spectral nudging. The method was described in detail in *Guldberg et al.* [2005]. The principle is to use a high resolution atmospheric model in which small scales can develop freely and large scales are driven by ERA40. The synoptic chronology then follows that of the reanalysis while the high resolution structures of the atmospheric flow are created by the model.

The ARPEGE-Climate model [*Déqué and Piedelievre*, 1995] is a global and spectral Atmosphere General Circulation Model whose grid can be stretched over the area of interest. We used a version with a pole located in the Tyrrhenian Sea and a resolution of ∼50 km over the Mediterranean Basin, as in *Sotillo et al.* [2005]. A nudging term was added to the equations of the temporal evolution of the prognostic variables (temperature, velocity and surface pressure). We chose a wavelength of 250 km as the limit of the waves driven by ERA40, and followed *Guldberg et al.* [2005] for e-folding times used for the nudging of the different variables. ERA40 fields were updated every 6 hours and linearly interpolated in between. The ARPEGE-Climate simulation covers the whole ERA40 period. Air-sea fluxes (water, heat and momentum) were extracted from both simulations (ERA40 reanalysis and ARPEGE-Climate simulation) and interpolated onto the ocean model grid (Section 3).

2.2. Comparison of atmospheric datasets

To underline the differences between the two datasets, we compared the new dynamical downscaling dataset (HRAF for High Resolution Atmospheric Forcing) with the initial

ERA40 dataset (LRAF for Low Resolution Atmospheric Forcing) over the Gulf of Lions. For this purpose, we examined the daily time series of the net heat loss (HL), net water loss (WL), buoyancy loss (BL) and wind stress (τ) averaged over the LION area (defined on Fig. 1c).

First, the spectral dynamical downscaling technique does not change the temporal chronology of the downscaled reanalysis. Indeed, both datasets are well correlated in time for τ, HL and WL (Fig. 1a). Each LRAF intense event is well represented in HRAF. Tab. 1 summarizes these correlations for the LION area over a wide winter period (December - April). Daily correlations are higher than 0.8 except for WL, due to the weaker ability of forced climate models to simulate the precipitation chronology [*Caya and Biner*, 2004]. This lower correlation for WL does not have a significant impact on the chronology of BL since BL is mainly driven by HL. Indeed, we computed a 0.99 time-correlation between BL and HL in both datasets, vs. 0.53, resp. 0.59 between BL and WL in LRAF, resp. HRAF.

Second, over the area of interest and for the winter period investigated, the dynamical downscaling slightly increases the winter average air-sea fluxes (Tab. 1).

Third, extreme air-sea fluxes during intense winter events are more pronounced in space and in time in HRAF than in LRAF. For HL, WL and BL, the value of the 90th percentile increases more than the time-averaged value (Tab. 1). This is even stronger for the maximum value. The upper end of the corresponding density functions increases consequently more than the average, as seen on the quantile-quantile plot for the three variables (Fig. 1b). This is also true for τ despite the inconsistent behavior of the maximum value which

is due to a slight temporal shift between HRAF and LRAF at the beginning of the E2 event (see Fig 1a). This very intense wind event is indeed concentrated in one day in LRAF but is split in two days in HRAF. A two-day average shows that HRAF is actually more windy than LRAF for this event. The upper end of the τ density function also increases more than the average (see Fig. 1b) even if the maximum value has a strong impact on the change of the 90th percentile value (Tab. 1). The lower end of the WL density function is explained by a rainier E2 event in LRAF than in HRAF, probably due to differences in model physics. The upper end of the density functions corresponds to the main synoptic weather events observed during this winter (LS91), characterized by regional Mistral or Tramontane winds (Fig. 1a). During these events, the impact of the resolution increases and the orography forcing becomes predominant in HRAF, leading to large differences with the initial reanalysis. Temporal extremes are therefore more pronounced in HRAF. The resolution enhancement also increases the intensity of small spatial scale structures in HRAF, as illustrated on Fig. 1c for a particular day. The relative difference in the HL winter mean between the MEDOC point (5°E, 42°N), known to undergo maximum heat loss, and the LION area is indeed equal to +12% in LRAF and +26% in HRAF.

Due to a lack of in-situ data, it is generally difficult to validate air-sea fluxes. For the 1986-87 winter, *Mertens and Schott* [1998] however provided values integrated from December to February: 2.5 10^9 J.m^{-2} for HL and 1.5 m^2.s^{-2} for BL. For HRAF (resp. LRAF), we obtained for the MEDOC point, 1.9 (resp. 1.6) 10^9 J.m^{-2} and 1.0 (resp. 0.85) m^2.s^{-2}.

Despite the large uncertainty associated to the *Mertens and Schott* [1998] data, HRAF dataset is closer to the observed data than LRAF.

3. Impact of atmospheric forcing resolution on deep convection modeling

We used the atmospheric datasets compared above to force a regional ocean model. Results of both simulations (HRAF and LRAF) were compared with data obtained during MEDOC87 to show the influence of atmospheric forcing spatial resolution on open ocean deep convection modeling and emphasize the interest of the downscaling method.

3.1. The oceanic model: SYMPHONIE

The 3D primitive equation eddy-resolving ocean model SYMPHONIE was used by *Herrmann et al.* [2008] to study the influence of the oceanic model spatial resolution on the modeling of the 1986-87 winter convection in the NWMS. We used the same configuration. This free-surface model is based on the hydrostatic assumption and the Boussinesq approximation. We used a 3-km orthogonal horizontal grid and a 40-level hybrid sigma-step coordinates system. Vertical diffusivities are calculated using the *Gaspar et al.* [1990] second-order closure scheme. In the case of unstable stratification a non-penetrative convective adjustment algorithm is used. At the surface, the model is forced by air-sea fluxes (heat, momentum and water flux). The water flux is the simple sum (without relaxation or correction) of the evaporation-minus-precipitation flux extracted from the ERA40 and ARPEGE-Climate atmospheric simulations, and of the Rhône river runoff (UNESCO RivDis database [*Vörösmarty et al.*, 1996] climatological monthly values). Two regional simulations were carried out between September 1986 and September 1987, forced with the LRAF and HRAF datasets respectively. The eddy-permitting oceanic model OPA

described in *Somot et al.* [2006] was used to perform two simulations over the whole Mediterranean sea using HRAF and LRAF air-sea fluxes. Monthly averaged results of each OPA simulation provided lateral boundary conditions and initial conditions for the regional simulations. The consistency of this forcing strategy was demonstrated in *Herrmann et al.* [2008].

3.2. Time evolution of the convection event

The LION area (Fig. 1c) entirely covers the convection zone. We examined the evolution of the maximum mixed layer depth (MLD_{max}) over the LION area during the 1986-87 winter for both simulations (Fig. 1a). As justified in *Herrmann et al.* [2008], the mixed layer depth was defined using a threshold value of 4 $cm^2.s^{-1}$ for the vertical diffusion coefficient. In LRAF MLD_{max} does not exceed 800 m: deep convection does not occur. In HRAF MLD_{max} begins to increase on 11th January and reaches 1200 m on 27th January. This first deepening is due to a mid-January intense Mistral event (E2, Fig. 1a), in agreement with the observations. By examining CTD and velocity profiles, LS91 and SL91 deduced that this event had initiated deep convection before 23rd January. During early February, MLD_{max} shallows to 500 m, as observed by LS91 and SL91. The third atmospheric event E3 induces a second deepening phase of the mixed-layer that reaches 1240 m on 23rd February. A brief but intense Mistral event (E4) occurs in the first few days of March after which MLD_{max} reaches the bottom. This represents a small delay (11 days) compared to LS91 and SL91 observations. MLD_{max} shallows to 1270 m, and then exceeds 2000m again after E5. Restratification begins on 26th March but is briefly interrupted by E6 until 5th April when it restarts once again. In HRAF, bottom

convection, corresponding to $MLD_{max} \geq 2000$ m, occurs and the mixed layer evolution is consistent with the atmospheric forcing and with the observations.

When bottom convection occurs, the water column is fully mixed and has homogeneous characteristics, corresponding to deep water (DW) temperature and salinity properties. DW characteristics observed by LS91 were 12.76°C, 38.44 psu, 29.11 kg.m^{-3}. In LRAF no deep convection occurs therefore no DW is formed, and the surface density never exceeds 29.06 kg.m^{-3}. Also using a 125 km resolution atmospheric forcing, *Demirov and Pinardi* [2007] obtained DW whose density did not exceed 29.05 kg.m^{-3} and attributed this to the low spatial resolution of the atmospheric forcing. In HRAF DW characteristics are 12.78°C, 38.44 psu, 29.10 kg.m^{-3}, similar to the observed values.

3.3. Deep convection spatial characteristics

LS91 defined the convection area as the region where sea surface salinity (SSS) exceeded 38.40 psu. The corresponding observed region on 21st February, when bottom convection occurred, is shown on Fig. 1d, as well as the mixed layer depth computed in LRAF on 8th February, when MLD_{max} is maximum, and in HRAF on 15th March, when bottom convection is established (Fig. 1a). In LRAF, as already observed, no deep convection occurs. In HRAF, though the convection area seems slightly underestimated, the size and position of this area, centered around (5°E, 42°N), is in better agreement with the observations.

Herrmann et al. [2008] carried out a simulation using corrected ERA40 fluxes: a 130 W.m^{-2} correction was added homogeneously to HL from December to February to correct its underestimation in ERA40. They obtained deep convection but the convection

area was too large and shifted to the southwest. This overestimation was very likely due to the homogeneity of the correction. The mean HL difference over the same period between LRAF and HRAF is indeed 20 W.m^{-2} for the LION area and 40 W.m^{-2} for the MEDOC point, respectively 70% and 85% smaller than the 130 W.m^{-2} correction: the downscaling method allows us to correct more accurately the atmospheric fluxes spatial and temporal extremes without overestimating HL over the entire region.

Thus, using downscaled ERA40 fluxes enables a more accurate representation of the size and position of the convection area and the characteristics of the DW formed than using raw or corrected ERA40 fluxes. Rather than an average increase in fluxes, the enhancement of meteorological extremes may be the determining factor in this improvement. Indeed, previous numerical studies showed that extreme atmospheric events [*Madec et al.*, 1991; *Artale et al.*, 2002] and space variability, through the strengthening of the wind stress curl [*Madec et al.*, 1996], promote deep convection.

3.4. Circulation during the convection event

The main current in the NWMS is the Northern Current that flows southwestward along the coast and across the Gulf of Lions shelf. In winter, it develops intense mesoscale meanders of a few tens of km [*Millot*, 1999]. For both simulations this current is visible on Fig. 1d. However, the current flowed steadily in LRAF, whereas in HRAF it is unstable with 30-50 km meanders. *Gascard* [1978] observed that mesoscale structures corresponding to baroclinic instabilities developed at the periphery of the convection area. Such meanders are present at the southern periphery of the convection in HRAF, but not in LRAF. In HRAF, they evolve into eddies of vertical scale larger than 1000 m, of radius

$\sim$ 10-15 km and of maximum orbital velocity $\sim$ 10 cm.s^{-1}. These eddies advect DW out of and stratified water into the convection area. These characteristics are in agreement with observations [*Gascard*, 1978; *Testor and Gascard*, 2006]. These structures play a major role during the convection event: they are responsible for the stabilization of the convection zone extension and DW characteristics, and contribute importantly to DW transport, therefore influencing the whole NWMS thermohaline circulation [*Testor and Gascard*, 2006; *Demirov and Pinardi*, 2007; *Herrmann et al.*, 2008]. The circulation during the convection event is therefore represented correctly in HRAF, and not in LRAF.

4. Conclusions

We chose the well-observed 1986-87 winter to evaluate the capacity of an eddy-resolving oceanic model forced by high resolution atmospheric fluxes to represent deep convection. Using ERA40 downscaling instead of directly using ERA40 fluxes, we obtained a better representation of the 1986-87 deep convection event: its temporal and spatial characteristics are in better agreement with the observations, and the circulation mesoscale processes, which play an essential role during deep convection, are accurately represented. To our knowledge, this is the first time that deep convection and associated mesoscale structures were simulated within a high-resolution realistic framework for both the oceanic model and the air-sea fluxes. This downscaling method enables us to correct the underestimation of spatial and temporal extreme air-sea fluxes in ERA40. As shown in this study, this appears to be crucial when modeling oceanic deep convection, a major circulation process in the NWMS. Detailed sensitivity tests should be performed to confirm this hypothesis. Other years and longer periods between 1958 and 2001 can now be studied using ERA40

downscaling, which provides an adequate high-resolution atmospheric forcing for modeling the Mediterranean thermohaline circulation and its interannual variability.

Acknowledgments. We would like to thank M. Déqué, C. Estournel, F. Sevault, M. Lucas and A. Pinari for their careful rereading and useful discussions.

References

Artale, V., D. Iudicone, R. Santoleri, V. Rupolo, S. Marullo, and F. D'Ortenzio (2002), Role of surface fluxes in ocean general circulation models using satellite sea surface temperature: Validation of and sensitivity to the forcing frequency of the Mediterranean thermohaline circulation, *J. Geophys. Res.*, *107 (C8)*.

Béranger, K., L. Mortier, and M. Crépon (2005), Seasonal variability of transports through the Gibraltar, Sicily and Corsica Straits from a high resolution Mediterranean model, *Prog. Oceanogr.*, *66*(2-4), 341–364.

Caya, D., and S. Biner (2004), Internal variability of rcm simulations over an annual cycle, *Clim. Dyn.*, *22(1)*, 33–46.

Demirov, E. K., and N. Pinardi (2007), On the relationship between the water mass pathways and eddy variability in the Western Mediterranean sea, *J. Geophys. Res.*, *112(C02024)*.

Déqué, M., and J. Piedelievre (1995), High-resolution climate simulation over Europe, *Clim. Dyn.*, *11*, 321–339.

Gascard, J.-C. (1978), Mediterranean deep water formation, baroclinic eddies and ocean eddies, *Oceanologica Acta*, *1(3)*, 315–330.

Gaspar, P., Y. Gregoris, and J. Lefevre (1990), A simple eddy kinetic energy model for simulations of the oceanic vertical mixing: tests at station Papa and long-term upper ocean study site, *J. Geophys. Res.*, *95*, 16,179–16,193.

Guldberg, A., E. Kaas, M. Déqué, S. Yang, and S. Vester Thorsen (2005), Reduction of systematic errors by empirical model correction : impact on seasonal prediction skill, *Tellus*, *57A*, 575–588.

Herrmann, M., S. Somot, F. Sevault, C. Estournel, and M. Déqué (2007), Modeling the deep convection in the Northwestern Mediterranean sea using an eddy-permitting and an eddy-resolving model: case study of winter 1986-87, *J. Geophys. Res.*, *in press*.

Josey, S. (2003), Changes in the heat and freshwater forcing of the Eastern Mediterreanean and their influence on deep water formation, *J. Geophys. Res.*, *108*(C7), 1–18.

Kalnay, E., et al. (1996), The NCEP/NCAR 40-year reanalysis project, *Bull. Amer. Meteor. Soc.*, *77*, 437–471.

Leaman, K. D., and F. Schott (1991), Hydrographic structure of the convection regime in the Gulf of Lions : winter 1987, *J. Phys. Oceanogr.*, *21*, 575–597.

Madec, G., M. Chartier, and M. Crépon (1991), The effect of thermohaline forcing variability on deep water formation in the Western Mediterranean sea: a high resolution three dimensional numerical study, *Dyn. Atm. Oceans*, *15*, 301–332.

Madec, G., F. Lott, P. Delecluse, and M. Crépon (1996), Large-scale preconditioning of deep-water formation in the Northwestern Mediterranean Sea, *J. Phys. Oceanogr.*, *26*, 1393–1408.

Mertens, C., and F. Schott (1998), Interannual variability of deep-water formation in the Northwestern Mediterranean, *J. Phys. Oceanogr.*, *28*, 1410–1424.

Millot, C. (1999), Circulation in the Western Mediterranean Sea, *J. Mar. Syst.*, *20*, 423–442.

Schott, F., and K. D. Leaman (1991), Observations with moored acoustic doppler current profilers in the convection regime in the Golfe du Lion, *J. Phys. Oceanogr.*, *21*, 558–574.

Simmons, A., and J. Gibson (2000), The ERA-40 project plan, ERA-40 project report series, *Tech. Rep. 1*, ECMWF, Shinfield Park, Reading, UK, 63pp.

Somot, S., F. Sevault, and M. Déqué (2006), Transient climate change scenario simulation of the Mediterranean Sea for the 21st century using a high resolution ocean circulation model, *Clim. Dyn.*, *27(7-9)*, 851–879.

Sotillo, M., A. W. Ratsimandresy, J. Carretero, A. Bentamy, F. Valero, and F. Gonzàlez-Rouco (2005), A high-resolution 44-year atmospheric hindcast for the Mediterranean Basin: contribution to the regional improvement of global reanalysis, *Clim. Dyn.*, *25*(2-3), 219–236.

Testor, P., and J.-C. Gascard (2006), Post-convection spreading phase in the Northwestern Mediterranean Sea, *Deep-Sea Res., Part I*, *53*, 869–893.

Vörösmarty, C., B. Fekete, and B. Tucker (1996), *Global river discharge database, RivDis*, UNESCO, Paris, international Hydrological Program, Global Hydrological Archive and Analysis Systems.

HRAF	mean	90th perc.	max.	corr.
HL	117 (+10%)	414 (+17%)	1042 (+58%)	0.91
WL	2.6 (+19%)	8.8 (+21%)	21.3 (+106%)	0.69
BL	6.5 (+11%)	22.1 (+15%)	57.1 (+68%)	0.88
τ	0.15 (+32%)	0.36 (+27%)	0.75 (-8%)	0.81

Table 1. HRAF values (mean, 90th percentile, maximum and time correlation with the LRAF time series) computed for the LION area from the daily values of the December-April period for the net heat loss (HL, W.m^{-2}), net water loss (WL, mm.day^{-1}), buoyancy loss (BL, 10^{-8} m^2.s^{-3}) and wind stress norm (τ, N.m^{-2}). The relative error between HRAF and LRAF datasets is given in brackets.

Figure 1. Atmospheric and oceanic characteristics during the 1986-87 winter for LRAF and LRAF. (a): Evolution of the mean wind stress τ, heat loss HL and water loss WL, and of the maximum mixed-layer depth MLD_{max} over the LION area between 01/12/86 and 30/04/87 for HRAF (red) and LRAF (black). Grey boxes mark meteorological events. (b): Quantile-quantile plot of τ, HL and WL averaged over the LION area. A loss for the sea corresponds to a positive value. (c): Total heat loss (W.m^{-2}, colors) and wind stress (N.m^{-2}, arrows) on 11/01/1987. The white line delineates the LION area. (d): Mixed layer depth (m, colors) and current at 50m depth (m/s, arrows) on 08/02/1987 for LRAF and on 15/03/1987 for HRAF. The black line delineates the observed convection area (LS91).

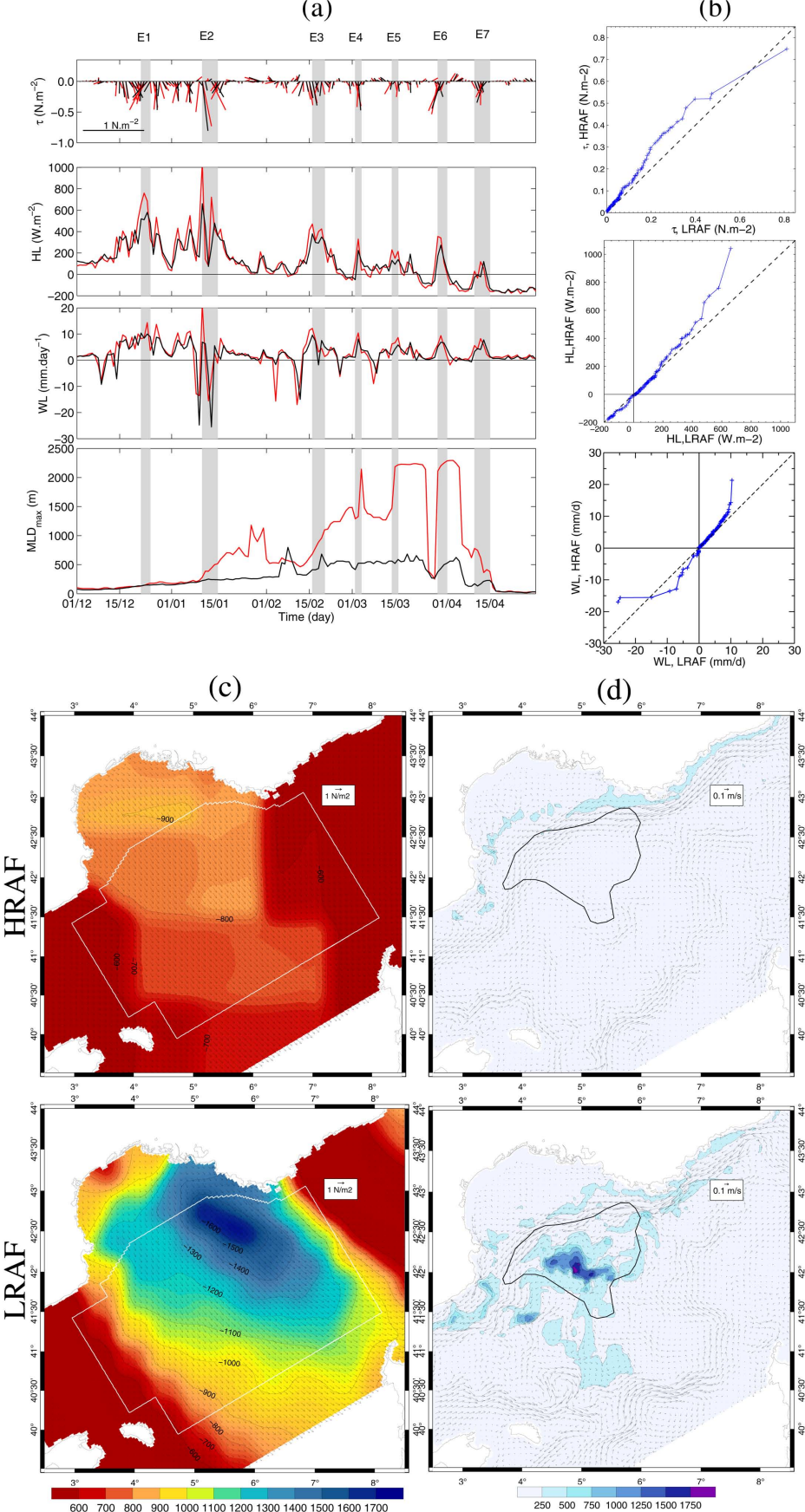
(a)
(b)
(c)
(d)
E1
E2
E3
E4
E5
E6
E7
τ (N.m−2)
1 N.m−2
HL (W.m−2)
WL (mm.day−1)
MLDmax (m)
01/12
15/12
01/01
15/01
01/02
15/02
01/03
15/03
01/04
15/04
Time (day)
τ, HRAF (N.m−2)
τ, LRAF (N.m−2)
HL,HRAF (W.m−2)
HL,LRAF (W.m−2)
WL, HRAF (mm/d)
WL, LRAF (mm/d)
HRAF
LRAF
1 N/m2
0.1 m/s
600 700 800 900 1000 1100 1200 1300 1400 1500 1600 1700
250 500 750 1000 1250 1500 1750